Synthesis, spectroscopic characterization (FT-IR, FT-Raman, and NMR), quantum chemical studies and molecular docking of 3-(1-(phenylamino)ethylidene)-chroman-2,4-dione

Edina H. Avdović, Dejan Milenković, Jasmina M. Dimitrić Marković, Jelena Đorović, Nenad Vuković, Milena D. Vukić, Verica V. Jevtić, Srećko R. Trifunović, Ivan Potočňák, Zoran Marković

PII: S1386-1425(18)30033-7
DOI: https://doi.org/10.1016/j.saa.2018.01.023
Reference: SAA 15742
To appear in: *Spectrochimica Acta Part A: Molecular and Biomolecular Spectroscopy*
Received date: 21 October 2017
Revised date: 6 January 2018
Accepted date: 9 January 2018

Please cite this article as: Edina H. Avdović, Dejan Milenković, Jasmina M. Dimitrić Marković, Jelena Đorović, Nenad Vuković, Milena D. Vukić, Verica V. Jevtić, Srećko R. Trifunović, Ivan Potočňák, Zoran Marković , Synthesis, spectroscopic characterization (FT-IR, FT-Raman, and NMR), quantum chemical studies and molecular docking of 3-(1-(phenylamino)ethylidene)-chroman-2,4-dione. The address for the corresponding author was captured as affiliation for all authors. Please check if appropriate. Saa(2017), https://doi.org/10.1016/j.saa.2018.01.023

Synthesis, spectroscopic characterization (FT-IR, FT-Raman, and NMR), quantum chemical studies and molecular docking of 3-(1-(phenylamino)ethylidene)-chroman-2,4-dione

Edina H. Avdović[a], Dejan Milenković[b], Jasmina M. Dimitrić Marković[c], Jelena Đorović[b], Nenad Vuković[a], Milena D. Vukić[a], Verica V. Jevtić[a], Srećko R. Trifunović[a], Ivan Potočňák[d], Zoran Marković[b,e*]

[a]University of Kragujevac, Faculty of Science, Department of Chemistry, Radoja Domanovića 12, 34000 Kragujevac, Republic of Serbia

[b]Bioengineering Research and Development Center, Prvoslava Stojanovića 6, 34000 Kragujevac, Republic of Serbia

[c]Faculty of Physical Chemistry, University of Belgrade, Studentski trg 12-16, 11000 Belgrade, Serbia

[d]Institute of Chemistry, P. J. Šafárik University in Košice, Moyzesova 11, 04154 Košice, Slovak Republic

[e]Department of Chemical-Technological Sciences, State University of Novi Pazar, Vuka Karadžića bb, 36300 Novi Pazar, Republic of Serbia

***Corresponding author's e-mail address: zmarkovic@np.ac.rs**

Abstract

The experimental and theoretical investigations of structure of the 3-(1-(phenylamino)ethylidene)-chroman-2,4-dione were performed. X-ray structure analysis and spectroscopic methods (FTIR and FT-Raman, ^{1}H and ^{13}C NMR), along with the density functional theory calculations (B3LYP functional with empirical dispersion corrections D3BJ in combination with the 6–311+G(d,p) basis set), were used in order to characterize the molecular structure and spectroscopic behavior of the investigated coumarin derivative. Molecular docking analysis was carried out to identify the potency of inhibition of the title molecule against human's Ubiquinol-Cytochrome C Reductase Binding Protein (UQCRB) and Methylenetetrahydrofolate reductase (MTHFR). The inhibition activity was obtained for ten conformations of ligand inside the proteins.

Keywords: Coumarine, NBO, Electrostatic potential, FTIR, NMR, Molecular docking

1. Introduction

Coumarine (benzopyran-2-one, or chromen-2-one) is naturally occurring substance with pleasant odor and bitter taste [1]. It was first isolated by A. Vogel from Tonka beans as early as 1820 [2]. A large number of coumarin derivatives are isolated from natural sources while some are synthesized in laboratories [3]. Coumarin and its derivatives are widespread in nature, especially in the world of plants [4,5]. Also, these compounds are found in the products of metabolism of microorganisms [6,7,8] and animals [9,10].

The coumarin is the simplest naturally occurring phenolic compound consisting of fused α-pyrone and benzene rings along with the carbonyl group on the pyrone ring at position 2 (Fig.1) [11]. The chemical behaviour of coumarin products is influenced by the presence of the lactone structure, the double bond of the α-pyrone and the aromatic ring. For example, under various conditions C3=C4 bond undergoes reduction to give chroman-2-ones [12]. Also, coumarin undergoes addition reactions, for example addition of Br_2 at C3=C4 bond, while in reaction with a Grignard reagent coumarin behaves as an electrophile.

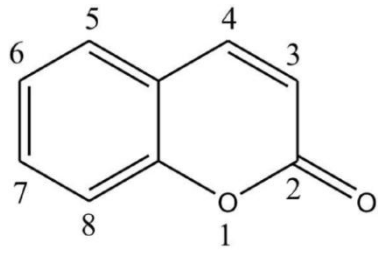

Figure 1. The chemical structure and numbering scheme of coumarin.

Because of their different chemical properties coumarin derivatives are important class of compounds and they have broad spectrum of pharmacological functions which include antibacterial [13, 14], antitumor [15], antioxidant [16], anti-inflammatory [17], anti-HIV [18], antifungal [3], antimutagenic [19] and inhibitory effects [20]. These compounds are also interesting for chemists because they are widely used: in fragrances and perfumes [21], as fluorescent probes [22], coumarin dyes [23], optical brighteners [24], molecular photonic devices [25], and as additives in food and cosmetics [26].

In accordance to above mentioned, the synthesis of coumarin derivatives attracts considerable attention and numerous techniques have been developed for their synthesis [22]. In our previously published paper [27], a coumarin derivative of **3**-(1-(2-hydroxyethylamino)-ethylidene)-chroman-2,4-dione was synthesized and its Pd complex showed good antitumor activity [27]. The 3-(1-(phenylamino)ethylidene)-chromane-2,4-dione (**1**) (Scheme 1) [28], was previously synthesized without spectroscopic and crystallographic details. In this paper the structure of the molecule is elucidated by using different spectroscopic methods (IR, ^{1}H NMR and ^{13}C NMR) in conjunction with the corresponding quantum chemical calculations at B3LYPD3BJ/6-311+G(d,p) level of theory, with the aim to examine the quality of the proposed DFT method and the possibilities of its application in the characterization of the structure of the **1** and other similar compounds. The proposed structure of the synthesized compound is also confirmed by using the X-ray structural analysis. The prepared compound **1** is investigated for the reactivity toward Ubiquinol-Cytochrome C Reductase Binding Protein (UQCRB) and Methylenetetrahydrofolate reductase (MTHFR) proteins by the means of the Molecular Docking analysis.

2. Experimental and Computational Methods

2.1. Chemicals and instrumentation

Starting compound, 3-acetyl-4-hydroxy coumarine, was synthesized in accordance to previously described procedure [29]. Aniline, methanol, toluene, acetone and 96 % ethanol were purchased from Sigma Aldrich (Munich, Germany).

The IR spectrum was recorded on the Perkin-Elmer Spectrum One FT-IR spectrometer (KBr pellet technique, 4000-400 cm^{-1}).

The NMR spectra (^{1}H NMR at 200 MHz and ^{13}C NMR at 50 MHz) were recorded on the Varian Gemini 200 spectrometer (Varian, Palo Alto, CA) with $CDCl_3$ as the solvent and TMS as the internal standard. Chemical shifts were given in δ (ppm), *J*-coupling constants in Hertz (Hz), abbreviations: s-singlet, dd-doublet of doublet, m-multiplet, br s-broadend singlet.

Elemental microanalysis for C, H and N was performed by using Vario EL III C, H, N Elemental Analyzer. Mass spectra were recorded on the 5973 Mass spectrometer (Agilent, Santa Clara, CA) (MS quadruple, temperature 150 °C; mass scan range, 40–600 amu at 70 eV). Analytical TLC was performed on silica gel (Silica gel 60, layer 0.20 mm, Alugram Sil G, Mashery-Nagel, Germany). Visualization of TLC plates was performed by using UV lamp at 254 nm and 365 nm (VL-4.LC, 365/254, Vilber Lourmat, France).

*2.2. **Synthesis and characterization of the title compound***

The synthesis of examined compound **1** was performed under similar conditions as previously described [27]. Briefly, a mixture of equimolar amounts of 3-acetyl-4-hydroxy

coumarine (0.4 g, 0.002 mol) and aniline (0.186 g, 0.002 mol) was refluxed for 1 hour in 50 ml of methanol. The reaction was monitored by TLC, by using solvent system toluene:acetone = 7:3 (v/v). At the end of reaction and after cooling to the room temperature, mixture was left in refrigerator overnight. The obtained white crystals were filtered, dried and recrystallized from 96 % ethanol. Yield: 0.49 g (87.5 %). *Anal*. Calcd. for $C_{17}H_{13}NO_3$ (*M* = 279.29 g/mol) (%): C, 70.95; H, 4.73; N, 4.87. Found: C, 70.77; H, 4.81; N, 4.79.

IR (KBr, cm^{-1}): 3425 (NH), 3046 (=CH), 2925, 2852 (CH), 1718 (C=O), 1609, 1590, 1561 and 1467 (C=C), 1192 (C-O).

^{1}H NMR ($CDCl_3$, 200 MHz) δ ppm: 2.69 (3H, s, C-1'-CH_3), 7.24 (2H, m, C-H-2", C-H-6"), 7.40 (1H, m, C-H-4"), 7.45 (2H, m, C-H-3", C-H-5"), 7.51 (2H, m, C-H-6, C-H-7), 7.57 (1H, m, C-H-8), 8.07 (1H, dd, $^3J_{H\text{-}5,\ H\text{-}6}$, H-6=7.99 Hz, $^4J_{H\text{-}5,\ H\text{-}7}$, H-7=1.98 Hz, C-H-5), 15.87 (br s, 1H, NH).

^{13}C NMR ($CDCl_3$, 50 MHz) δ ppm: 20.67 (C-1'-CH_3), 97.88 (C-3), 116.52 (C-8), 120.01 (C-6), 123.53 (C-5), 125.54 (C-10), 125.99 (C-4"), 128.18 (C-3" and C-5"), 129.57 (C-2" and C-6"), 134.05 (C-7), 136.17 (C-1"), 153.78 (C-9), 162.26 (C-2), 175.92 (C-1'), 181.74 (C-4).

M^+ m/z (%) = 279 (84 %).

*2.3. **X–ray data collection and structure refinement***

A summary of X-ray diffraction experiment and structure refinement for **1** is given in Table 1. The data collection was performed on an Oxford Diffraction Xcalibur2 diffractometer equipped with a Sapphire2 CCD detector with graphite-monochromatized MoKα radiation (λ = 0.71073 Å). Crysalis CCD [30] was used for data collection while Crysalis RED [30] was used for cell refinement, data reduction and absorption correction. The structure was solved by

SHELXT [31] and subsequent Fourier syntheses using SHELXL [32], implemented in WinGX program suit [33]. Anisotropic displacement parameters were refined for all non-hydrogen atoms. The hydrogen atom of amine group was found in the Fourier map and refined freely, carbon bonded hydrogen atoms were placed in the calculated positions and refined riding on their parent C with corresponding C–H distances and *U*iso(H) = 1.2 or 3.5 *U*eq(C). The analysis of bond distances and angles as well as nonbonding interactions was performed using SHELXL and PLATON [34]. DIAMOND [35] was used for molecular graphics.

Table 1. Crystal data and structure refinement for **1**.

Empirical formula	$C_{17}H_{13}NO_3$
Formula weight	279.28
Temperature	173(2) K
Wavelength	0.71073 Å
Crystal system	Monoclinic
Space group	$P2_1/c$
Unit cell dimensions	a = 11.2682(6) Å
	b = 16.5276(11) Å β = 102.323(5)°
	c = 7.2379(4) Å
Volume	1316.90(14) Å^3
Z	4
Density (calculated)	1.409 Mg/m^3
Absorption coefficient	0.097 mm^{-1}

$F(000)$	584
Crystal size	0.6068 x 0.1345 x 0.1088 mm^3
θ range for data collection	3.133 to 26.500°
Index ranges	$-14 \leq h \leq 13$, $-20 \leq k \leq 18$, $-9 \leq l \leq 9$
Reflections collected	5423
Independent reflections	2712 [R(int) = 0.0154]
Completeness to θ = 25.242°	99.8 %
Absorption correction	Analytical
Max. and min. transmission	0.990 and 0.977
Refinement method	Full-matrix least-squares on F^2
Data / restraints / parameters	2712 / 0 / 195
Goodness-of-fit on F^2	1.035
Final R indices [$I > 2\sigma(I)$]	$R1$ = 0.0422, $wR2$ = 0.0948
R indices (all data)	$R1$ = 0.0635, $wR2$ = 0.1081
Largest diff. peak and hole	0.190 and -0.211 e.$Å^{-3}$

2.4. Theoretical calculation

Theoretical calculations of the title compound **1** were carried out with Gaussian 09 software program [36] at the B3LYP-D3BJ/6-311G+(d,p) level. Calculations were done with the global hybrid Generalized Gradient Approximation (GGA) functional B3LYP [37-39], with empirical D3BJ dispersion corrections (with Becke and Johnson damping) [40-42] and empirical correction term proposed by Grimme [41,42], in combination with the 6–311+G(d,p) basis set. The B3LYP-D3BJ, which has been successfully used by independent authors [43,44], was

selected as a widely applicable method that proved to describe interatomic interactions at short and medium distances (≤5 Å) more accurately and reliably than traditional DFT methods. This optimization was performed to reproduce the structure obtained by the X-ray analysis.

The structure was optimized at 298 K without any geometrical restrictions. The nature of the stationary points was determined by performing frequency analysis: equilibrium geometries have no imaginary vibrations. To predict the IR and Raman spectra the geometry optimized in gas-phase was used. The vibrational modes of **1** were assigned on the basis of the PED (Potential Energy Distribution) analysis [45] using the FCART version 7.0 software [46]. In geometry optimization and energy calculations the effect of the solvent was taken into account by employing the SMD model [47]. The optimized structure in chloroform solution was used to simulate the NMR at same level of theory. The ^{1}H and ^{13}C NMR chemical shifts of **1** were predicted by means of the GIAO (Gauge Independent Atomic Orbital) method [48], as implemented in Gaussian 09. The NBO analysis was performed by using the NBO 5.9 software [49, 50].

The molecular docking simulation was carried out with the AutoDock 4.0 software [51]. The three-dimensional crystal structures of UQCRB and MTHFR proteins were obtained from the Protein Data Bank (PDB IDs: 1BCC and 1V93) [52,53]. The Discovery Studio 4.0 was used for preparation of protein for docking by removing the co-crystallized ligand, water molecules and co-factors. In order to calculate Kollman charges and to add the polar hydrogen the AutoDockTools (ADT) graphical user interface was used. Title molecule (3) (Fig.2b) was prepared for docking by minimizing its energy at B3LYP-D3BJ/6-311+G(d,p) level of theory. The flexibility of the ligands was considered, while the protein or biomolecules remained as rigid structure in the ADT. All bonds of **1** were set to be rotatable. The Geistenger method for

calculation of partial charges was employed. All calculations for protein - ligand flexible docking were done using the Lamarckian Genetic Algorithm (LGA) method. The grid boxes with dimensions 38.081×106.699×63.749 of UQCRB and 85.786×105.442×64.873 of MTHFR proteins could cover all of the protein binding sites and accommodate ligand to move freely. Inhibition potency of the title molecule was investigated and discussed for several most stable conformations.

3. Results and discussion

3.1. Chemical synthesis

The refluxing of equimolar amounts of 3-acetyl 4-hydroxy coumarine and aniline in methanol led to the formation of chroman-2,4-dione derivative (**3**) in a yield of 87.5 % (Scheme 1). Compound **1** was previously synthesized, but without sufficient spectroscopic data [28].

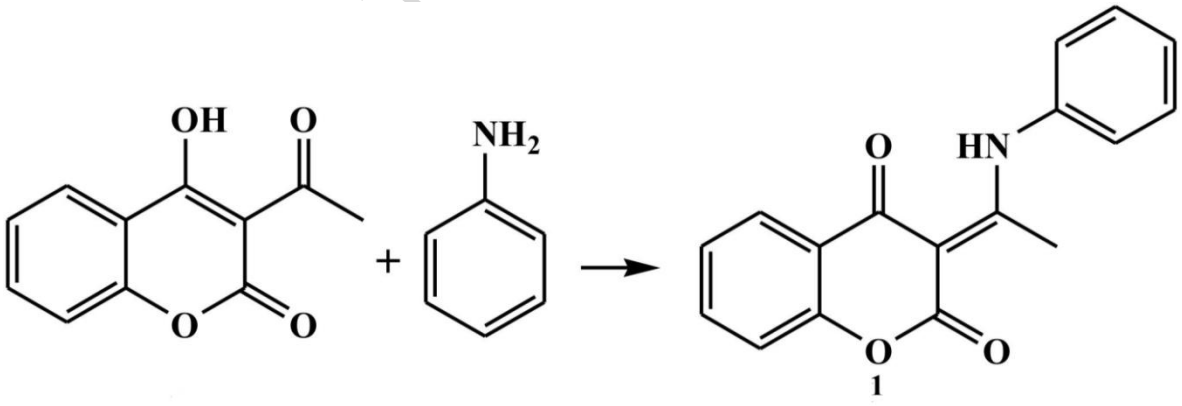

Scheme 1. Synthesis of the 3-(1-(phenylamino)ethylidene)chroman-2,4-dione, **1**.

3.2. Single crystal X-ray diffraction and molecular geometry

X-ray structure analysis of **1** was performed and details are presented in following paragraphs. The bond lengths and angles for **1** are presented in Table 2 and S1. The molecule (3) consists of the bicyclic coumarine fragment and the phenyl ring joined by aminoethylidine chain (Fig. 2a) with dihedral angle between the planes of coumarine fragment and phenyl ring being 45.62(3) °, which is very similar to the values observed in the above mentioned toluidine-isomers.

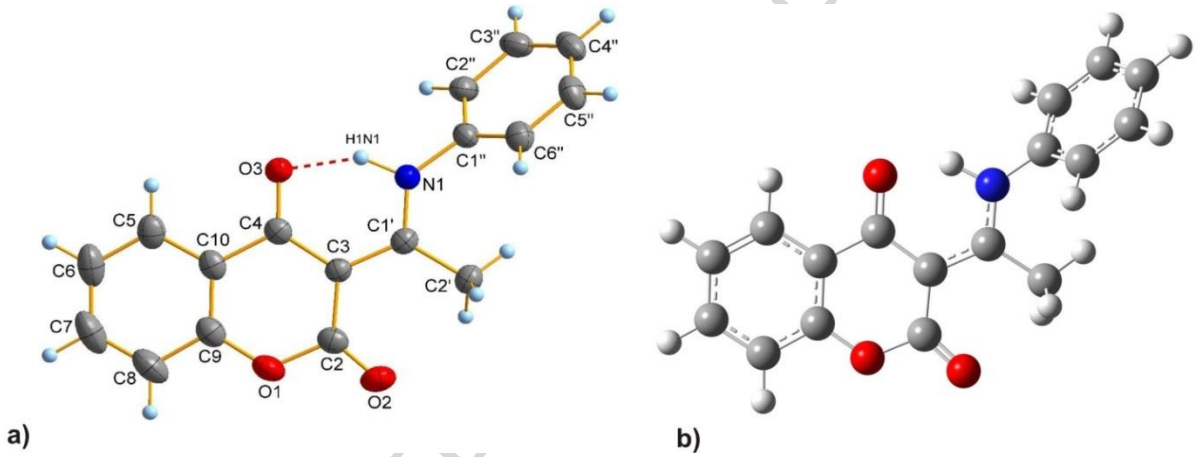

Figure 2. Molecular structures with atom numbering scheme of **1**. a) X-Ray structure; b) the optimized structure obtained at the B3LYP-D3BJ/6–311+G(d,p) level of theory.

Typical structural feature of that type of compounds is an intramolecular N−H···O hydrogen bond which forms a six-membered ring with S(6) graph set motif [54] determining the keto-amine tautomeric form of the molecule. Considering the O3=C4−C3=C1'−N1−H1 conjugated bond ring system, created owing to the intramolecular hydrogen bond formation, the equalization of the C3−C4 (1.435(2) Å) and C3=C1' (1.425(2) Å) bond lengths (Table 2) can be observed, although the bonds are formally single and double, respectively. This could be explained by the π-electron delocalization within the system and thus it can be concluded that

above hydrogen bond can be classified as a resonance assisted hydrogen bond [55]. Interestingly, in above mentioned 3-(1-((m-toluidine)amino)ethylidene)-chroman-2,4-dione and in the related 3-(1-(2-hydroxyethylamino)ethylidene)-chroman-2,4-dione [56] compounds, C3−C4 bonds were even slightly shorter than C3=C1' bonds. The elongation of C4=O3 (1.259(2) Å) bond could be also observed and it was markedly longer than C2=O2 (1.204(2) Å) bond but not involved in a strong hydrogen bond. The shortening of C1'−N1 (1.322(2) Å) bond in **1** was also noted. Very similar bond lengths were observed in related compounds mentioned above as well as in others, like 3-(1-(3-hydroxypropylamino)propylidene)chroman-2,4-dione [57], 2-(1-(2,4-dioxochroman-3-ylidene)ethylamino)-3-methylbutanoate [58], 3-[(1-benzylamino)ethylidene]-2*H*-chromene-2,4(3*H*)-dione [59] or in 3-[1-((2-hydroxyphenyl)amino)ethylidene)-2*H*-chromene-2,4(3*H*)-dione compound [60]. All other bond lengths and angles in the molecule of **1** were within normal ranges [61].

Except above discussed N1−H···O3 intramolecular hydrogen bond, due to which the exocyclic C3=C1' double bond had an *E* geometry, the molecules of **1** were stabilized in the solid state by weaker intermolecular C−H···O hydrogen bonds (Table 3). Due to these bonds the molecules of **1** were tied to form a chain along the *c* axis (Fig. 3). No significant interactions between individual chains could be found.

Table 2. The bond lengths (Å) in neutral molecule, optimized with B3LYP-D3BJ/6-311+G(d,p) model (the atom numbering is in line with Fig. 2). Experimental values are also included.

Bond lengths (Å)	Experimental	Calculated
	1	**1**
D(O1–C2)	1.388(19)	1.391
D(C2–C3)	1.453(2)	1.459
D(C3–C4)	1.435(2)	1.452
D(C4–C10)	1.466(2)	1.468
D(C10–C5)	1.390(2)	1.403
D(C5–C6)	1.379(2)	1.384
D(C6–C7)	1.378(3)	1.401
D(C7–C8)	1.371(3)	1.387
D(C8–C9)	1.387(2)	1.395
D(C9–C10)	1.378(2)	1.394
D(C9–O1)	1.370(2)	1.363
D(C3–C1')	1.425(2)	1.422
D(C1'– C2')	1.487(2)	1.499
D(C1'– N1)	1.322(18)	1.334
D(N1–C1")	1.434(18)	1.419
D(C1"– C2")	1.383(2)	1.396
D(C2"– C3")	1.382(2)	1.392
D(C3"– C4")	1.381(2)	1.394
D(C4"– C5")	1.382(2)	1.394

D(C5"– C6")	1.383(2)	1.391
D(C6"– C1")	1.384(2)	1.397
D(C2–O2)	1.204(18)	1.209
D(C4–O3)	1.259(17)	1.250
D(N1–H)	1.000(18)	1.041
D_H(N1–H···O3)	1.631(18)	1.629

D_H hydrogen bond

Table 3. Hydrogen bonds for **1** [Å and °].

D–H···A	*d*(D-H)	*d*(H···A)	*d*(D···A)	<(DHA)
C2'–H2'C···O3	0.98	2.58	3.25(18)	126.0
C6"–H6"···O3	0.95	2.60	3.30(19)	130.2
N1–H···O3	1.00(2)	1.63(2)	2.53(17)	147.0(16)

Symmetry transformations used to generate equivalent atoms: (i): *x*, -*y* + 1.5, *z* + ½; (ii): *x*, -*y* + 1.5, *z* – ½.

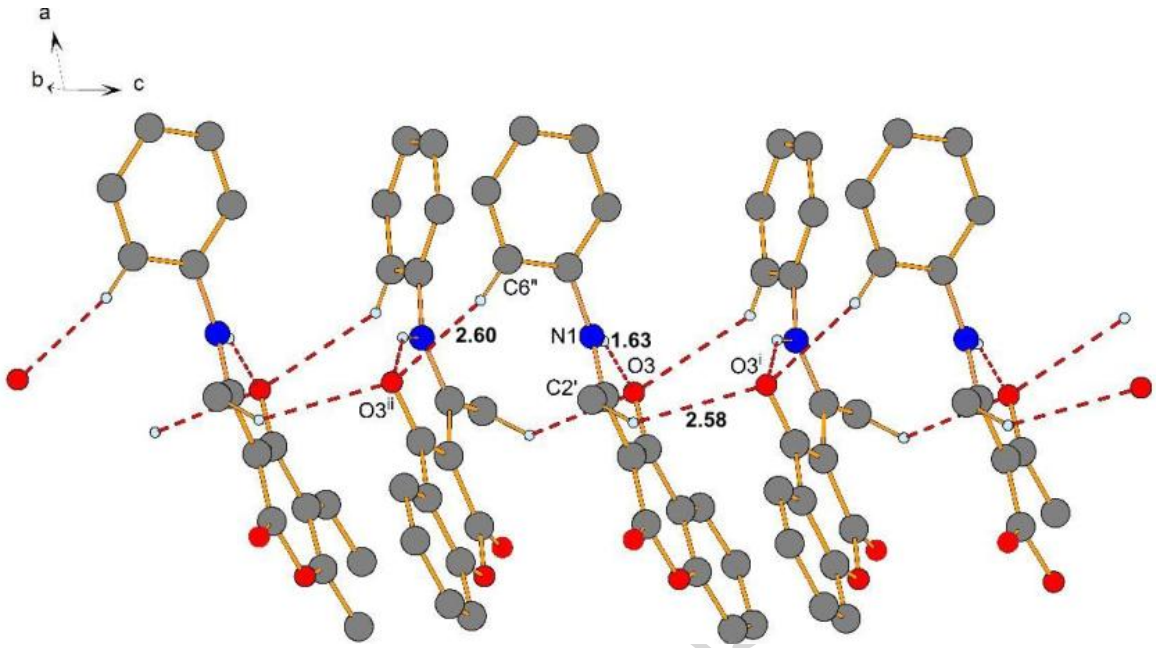

Figure 3. Crystal structure of **1** showing hydrogen bonds (red dashed lines) forming a chain along the *c* axis. Hydrogen atoms not involved in hydrogen bonds are omitted for clarity. Symmetry codes: (i): *x*, -*y* + 1.5, *z* + ½; (ii): *x*, -*y* + 1.5, *z* – ½. The most important interaction distances (bold) are given in angstrom (Å).

3.3. Molecular geometry of examined compound 1

The geometry of ligand, as optimized at B3LYP-D3BJ/6–311+G(d,p) level of theory, is depicted in Fig. 2b. The calculated bond lengths and angles are given in the same tables as experimental. The theoretical and experimental data indicated that molecule **1** was non-planar (Table S1). The C6"–C1"–N1–C1' torsion angle (τ) determined by the X-ray study and DFT methods yielded to the same value of 52.4°. The difference between the bond lengths of **1,** obtained by crystallographic analysis and theoretical calculations, amounted to 0.87%. It is evident that B3LYP-D3BJ level of theory reproduces the bond lengths of molecule **1** excellently.

The obtained correlation coefficient and the absolute errors are 0.996 and 0.01 Å, respectively (Table 2).

3.4. Vibrational spectra

The synthesized coumarin derivative possesses low symmetry due to which its FT-IR and Raman spectra were quite similar in appearance. More bands were present in the IR spectrum which is a consequence of the Raman scattering effect itself.

In the high frequency region (4000 – 2000 cm^{-1}) (Table S2) bands were assigned to different C–H stretching modes of both rings. According to PED values (Table S2) the region between 3200-3060 cm^{-1} was assigned solely to C–H stretching modes (99-92%). The rest of the modes were presented as the combination of various contributions.

Below 2000 cm^{-1}, between 2000-1000 cm^{-1}, very strong and strong bands at 1718 (IR), 1609 (IR), 1613 (R), 1587 (R), 1590 (R), 1559 (IR) and 1479 (R) are assigned to C=O stretching modes of pyrone ring, N–C and C–C stretching and C–N–H bending modes. Bands at 1480 (IR), 1479 (R), 1468 (IR), 1465 (R), 1449 (IR) and 1424 (IR) cm^{-1}, also very strong to medium in intensity, are assigned to C–C stretching modes of the benzene ring (the second ring attached to N atom), H–C–C and H–C–H (-CH_3 (a)) bending modes. Strong to medium bands at 1341 (IR), 1336 (R), 1318 (R), and 1246 (R) belong to different combinations of bending and torsion (C–C–C, C–C–O and C–C–N–H) modes as well as combination of stretching and bending modes (C–C, C–C–C and C–C–H). Below 1200 cm^{-1} very strong to medium bands at 1246 (R), 1190 (IR), 1179 (IR), 1155 (IR), 1032 (IR) and 1006 (R) cm^{-1} belong to different bending (C–N–H, C–C–C, H–C–C) modes of both rings and the alkyl chain and to C–C and C–N stretching modes as well. In this same range, between 2000-1000 cm^{-1}, there are also some weak modes, at 1370 (IR),

1310 (IR), 1288 (IR), 1238 (IR), 1200 (R), 1180 (R), 1162 (IR, R) and 1075 (IR, R) cm^{-1}, assigned mostly to H–C–C bending and C–C stretching modes of both the rings.

In the low frequency regions, below 1000 cm^{-1}, of both IR and Raman spectra there are mostly weak bands assigned to H–C–C–H, O–C–C–C, C–C–C–C and C–C–N–H torsion modes of both rings (878 (IR), 845 (R), 761 (IR), 743 (IR), 707 (IR), 690 (IR), 576 (R), 508 (IR) cm^{-1}).

The results from Table S2 show that there is a linear dependence between the experimental and the calculated wavenumbers. The quality of this linear correlation is evaluated by means the correlation coefficient (R). The both R values for the IR and Raman spectra are 0.999. On the basis of these facts, it can be concluded that B3LYP-D3BJ provides very good agreement between the experimental and simulated vibrational spectra [62], indicating correct mode assignments (Fig. 4 and S1).

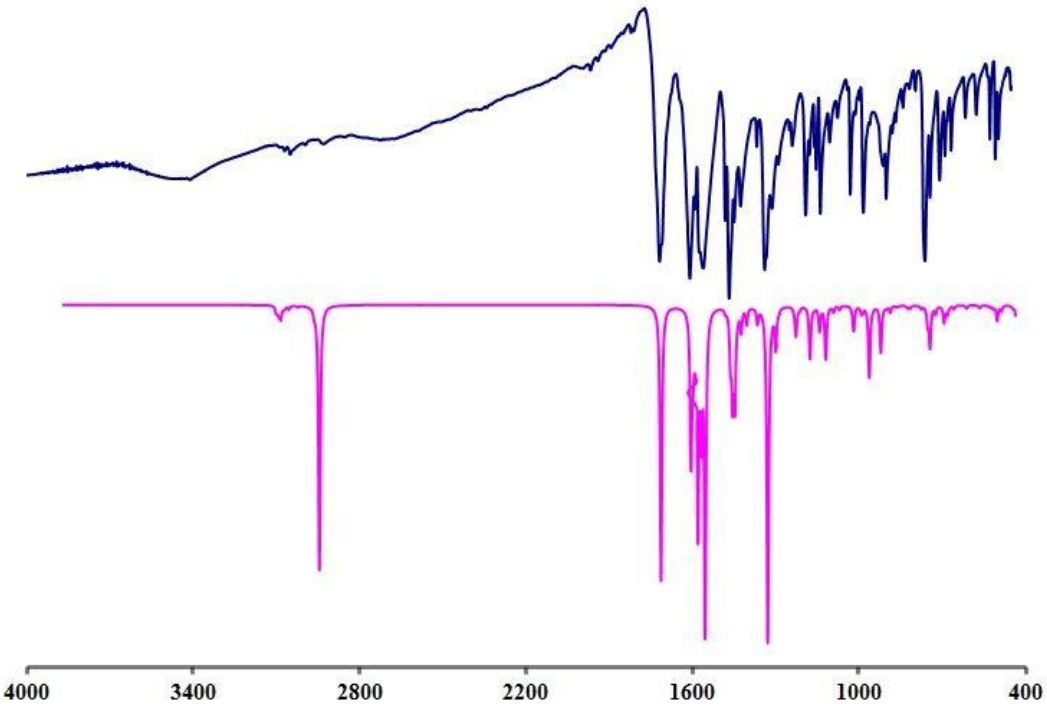

Figure 4. The experimental (blue line) and simulated (pink line) IR spectrum of **1**.

3.5. NMR spectra

The experimental ^{1}H and ^{13}C NMR spectra of **1** were obtained in chloroform and they are used to confirm the molecular structure in the solution. The experimental and calculated ^{1}H NMR and ^{13}C NMR chemical shifts are presented in Tables 4 and 5 (the atom numbering is in line with Fig. 2).

Table 4. Calculated and experimental ^{1}H chemical shifts (ppm) of selected protons bonded to the carbons.

	Experimental	**Calculated**
Compound	**1**	**1**
$C(2')H_3$	2.69	2.70
C(2")H	7.24	7.73
C(3")H	7.45	7.87
C(4")H	7.40	7.63
C(5")H	7.45	7.82
C(6")H	7.24	7.62
C(6)H	7.51	7.65
C(7)H	7.51	8.02
C(8)H	7.57	7.60
C(5)H	8.07	8.52
N(1)H	15.9	15.8
Mean absolute error (MAE)		0.28
R		0.998

Table 5. Calculated and experimental ^{13}C chemical shifts (ppm) of selected carbons.

^{13}C NMR	**Experimental**	**Calculated**
Compound	**1**	**1**
C(1')	175.9	177.1
C(2')	20.67	17.33
C(1'')	136.2	138.6
C(2'')	129.6	125.7
C(3'')	128.2	130.4
C(4'')	126.0	127.5
C(5'')	128.2	129.1
C(6'')	129.6	126.9
C(2)	162.3	161.6
C(3)	97.88	98.2
C(4)	181.7	182.8
C(5)	123.5	126.9
C(6)	120.0	123.0
C(7)	134.1	135.1
C(8)	116.5	116.3
C(9)	153.8	156.8
C(10)	125.5	120.0
Mean absolute error (MAE)		2.14
R		0.998

It is known that ^{1}H NMR spectra of organic molecules vary greatly depending on the electronic environment of the corresponding proton. The proton nearby electron-donating atom or group is more shielded, while the proton nearby electron-withdrawing atom or group is less shielded. It means that δ values will move to lower or higher values, respectively. The values of the chemical shift for aromatic protons are usually in the interval between 7-8 ppm. The experimental values for the nine aromatic protons of **1** were in the interval of 7.24-8.07 ppm while the corresponding theoretical values lied in the interval 7.60-8.52 ppm. The broad singlet at 15.9 ppm indicated the enamine N–H group (assigned to N(1) atom). The experimental chemical shift value of the protons of the methyl group was 2.69 ppm while the calculated value was 2.70 ppm (Table 4).

In the case of ^{13}C NMR spectrum of **1,** the experimental chemical shifts for aromatic carbons were in the range 120.0-153.8 ppm, while the calculated values were in the range 120.0-156.8 ppm. These values are a good match with the well-known fact that the chemical shifts values of the aromatic carbons lie in the range 100-150 ppm. Higher value of the chemical shift for C9 is expected due to adjacent of O1 atom. The difference in the chemical shift values for other carbons: C(1'), C(2), and C(4) is due to the positioning of these carbons with respect to adjacent electronegative atoms (N and O atoms) (Table 5).

The calculated and experimental chemical shift (Figs. S2 and S3) values given in Tables 4 and 5 show moderately large correlation coefficients and small mean absolute errors. According to the R and MAE values, the B3LYP-D3BJ method shows comparable ability to simulate the NMR spectrum of compound **1**.

3.6. NBO analysis

The NBO analysis was used for the investigation of electronic structure of the molecule **1**. In order to evaluate the donor–acceptor interactions in the NBO basis, the second-order perturbation theory analysis of Fock matrix was performed. The interactions resulted in a loss of occupancy from the localized NBO of the Lewis structure into an empty non-Lewis orbital. For each donor (*i*) and acceptor (*j*) the stabilization energy (*E*(2)) associated with the delocalization between *i* and *j* was determined as:

$$E(2) = \Delta E_{ij} = q_i \frac{(F_{ij})^2}{\left(E_j - E_i\right)} \quad (1)$$

where q_i was the donor orbital occupancy, E_i, E_j were diagonal elements (orbital energies) and $F_{i,j}$ was the off diagonal NBO Fock matrix element. The NBO analysis is an efficient method for investigating the hyperconjugative interaction or charge transfer (CT) in molecular systems. It should be noted that the higher value of *E*(2) represents the more intensive interaction between electron donors and electron acceptors. The second-order perturbation theory analysis of Fock matrix in the NBO basis of the molecule showed strong intramolecular hyperconjugative interactions which are presented in Table 6.

Table 6. Some selected second order interaction energies for **1.**

Donor(*i*)	ED/e	Acceptor(*j*)	ED/e	$E(2)$/kJ mol^{-1}	$E(j)$-$E(i)$/a.u.	$F(i,j)$/a.u.
πC3–C1'	1.64	π*O3–C4	0.35	159.87	0.26	0.090
πC3–C1'	1.64	π*O2–C2	0.31	140.00	0.27	0.087
πC9–C10	1.63	π*O3–C4	0.35	109.62	0.27	0.075
πC9–C10	1.63	π*C5–C6	0.28	83.51	0.30	0.071
πC9–C10	1.63	π*C7–C8	0.31	65.48	0.29	0.061
πC5–C6	1.68	π*C9–C10	0.41	72.01	0.28	0.063
πC5–C6	1.68	π*C7–C8	0.31	93.22	0.28	0.071
πC7–C8	1.69	π*C9–C10	0.41	95.40	0.28	0.073
πC7–C8	1.69	π*C5–C6	0.28	67.91	0.29	0.062
LP2 O3	1.86	σ*N1–H	0.08	105.35	0.68	0.119
LP2 O3	1.86	σ*C3–C4	0.05	46.19	0.78	0.085
LP2 O3	1.86	σ*C4–C10	0.06	70.88	0.76	0.103
LP2 O1	1.76	π*O2–C2	0.31	144.35	0.34	0.099
LP2 O1	1.76	π*C9–C10	0.41	124.98	0.35	0.096
LP2 O2	1.83	σ*O1–C2	0.11	148.28	0.57	0.128
LP2 O2	1.83	σ*C2–C3	0.06	67.99	0.71	0.098

The analysis of Fock matrix implicated the strong intermolecular hyperconjugative interactions between n(O) and σ *(N–H), σ*(O–C), π*(C–O), π*(C–C), between π(C–C) and π*(C–C), π*(O–C) orbitals which resulted in an intramolecular charge transfer (ICT) causing stabilization of the investigated compound.

The electron donation from the bonding π(C3–C1') to anti-bonding acceptor orbital π*(O3–C4) had the highest value of the interaction energy (Table 6). Also, the strong interaction energy between the bonding π(C3–C1') to anti-bonding orbital π*(O2–C2) was observed.

In addition, there were strong intermolecular hyperconjugative interactions from (LP2) O1 to π*(C2–O2) and π*(C9–C10), and from (LP2) O2 to σ*(C2– O1). The relatively strong electron donation from the π(C–C) orbitals to the π*(C–C) orbitals of the both aromatic rings was found. There were intramolecular hyperconjugative interactions between π(C–C) and π*(C–C) orbitals in the ring attached to pyron moiety which resulted in an ICT causing stabilization of the system. These interactions were followed by an increase in electron density (ED) in the C–C antibonding orbitals. The obtained values for ED of about 1.7e clearly showed strong delocalization of electrons which lead to the additional stabilization of the structure by the amount of ~65–95 kJ mol^{-1}. It should be noted that there was strong intermolecular hyperconjugative interaction between π(C9–C10) and π*(C4–O3) orbitals, which lead to stabilization of 109.6 kJ mol^{-1}. Strong hydrogen bond (1.63 and 1.24 Å measured and calculated values) was formed between N1–H···O3. This is inspected result, since it is well known that the NH groups are good hydrogen bond donors. On the other hand, the electron pairs on the oxygen of the C=O groups were much better hydrogen bond acceptors than the oxygen of the OH groups. The NBO analysis revealed that the ED was donated from the *p* orbitals of the oxygen atom O3 into the proximate σ* antibonding N1–H bond (Table 6). This hydrogen bond additionally stabilized the structures with 105.4 kJ mol^{-1}.

3.7. Molecular electrostatic potential analysis

The molecular charge distribution was represented by the map of the electrostatic potential (MEP). This map provided a visual method to understand the charged regions as well as the relative polarity of a molecule [63, 64]. On the basis of this map is possible to depict the shape and size, as well as the charge density and site of the chemical reactivity of the investigated molecules. The MEP of title compound presented in Fig. 5a, clearly indicates that the chromane's oxygen atom 1 as well as carbonyl oxygen atoms 2 and 3 contribute to the most electronegative region (red). Due to the excess negative charge, one can expect a relatively high nucleophilic activity of this part of the molecule. This is consistent with the well-known fact that the negative regions of MEP are usually associated with the lone electron pairs belonging to the electronegative atoms in the molecule. On the other hand, the positive values of MEP were localized over the hydrogen atoms bonded to oxygen atom.

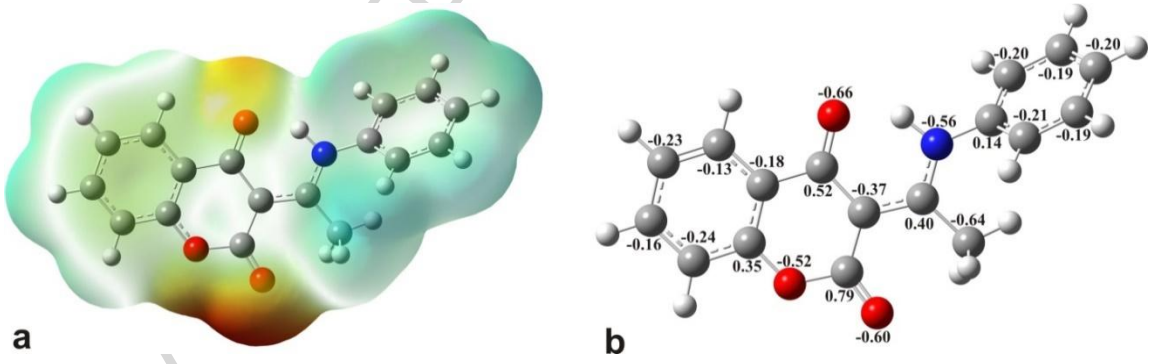

Figure 5. Molecular electrostatic potential surface (left) and the natural charge distribution (right).

The obtained values of the natural charge distribution are presented in Fig. 5b. The obtained results were in accordance with MEP data. As expected, the negative charge was manly distributed over the oxygen atoms attached to the chromane part while the rest of the negative natural charge was mostly delocalized over the C2', N1 and benzene rings. The C2 atom had greater positive charge than other C atoms in chroman part of the molecule (C4 and C9), as well as adjacent carbon atom C1'. In addition, slightly positive natural charge was almost uniformly distributed over hydrogen atoms.

3.8. Non-linear optical properties

To predict the non-linear optical (NLO) activity of the title molecule the components of various electric moments such as dipole moment (μ), polarizability (α) and first order static hyperpolarizability (β) were calculated using the DFT/B3LYP-D3BJ/6-311+G(d,p) method. The polarizability and the first hyperpolarizability (β) were calculated using the finite-field approach. The total electric dipole moment (μ_{total}), mean polarizability (α_{mean}) and the total first order static hyperpolarizability (β_{total}), were calculated using the x, y, and z components of these electric moments [65] (Table S3).

In present case, the calculated total dipole moment of the molecule under investigation was 3.62 Debye. The predicted value of the mean polarizability (α_{mean}) and total first order static hyperpolarizability (β_{total}) were found to be 34.934×10^{-24} esu and 6.484×10^{-30} esu, respectively. The calculated value of β_{total} for **1** was thirty times higher than that of Urea (0.1947×10^{-30} esu) [65], which is one of the prototypical molecules used in the study of the NLO properties of different molecular systems, frequently used as a threshold value for comparative purposes. It is

known that the high polarizability of the investigated compound implicates its drug-likeliness, as a result of high polarizability, which allows very strong binding with its target.

3.9. Fukui functions

Fukui functions, proposed by Parr and Yang in 1984 [66-68], are described as the change in total electron density on the basis of change in total number of electrons. Fukui functions can be calculated using the following equation:

$$f(r)=\left[\frac{\delta\mu}{\delta\upsilon(r)}\right]_N=\left[\frac{\partial\rho(r)}{\partial N}\right]_{\upsilon(r)}$$

(2)

where μ and N are the chemical potential and the number of electrons in the system, $v(r)$ is the external potential. The Fukui function can be approximated using following equations:

$$f^{-}(r)=\rho_N(r)-\rho_{N\text{-}1}(r)\approx\rho^{\mathrm{HOMO}}(r) \quad (3)$$

$$f^{+}(r)=\rho_{N+1}(r)-\rho_N(r)\approx\rho^{\mathrm{LUMO}}(r) \quad (4)$$

$$f^{0}(r)=\left[f^{-}(r)+f^{+}(r)\right]/2\approx\left[\rho^{\mathrm{HOMO}}(r)+\rho^{\mathrm{LUMO}}(r)\right]/2 \quad (5)$$

The evaluation of these equations can be very complicated due to the electron density term [69]. In equations 3-5, the frozen-orbital approximation is assumed. Parameters ρ_N(r), ρ_{N-1}(r) and ρ_{N+1}(r) separately represent the electron densities of the system with N (neutral molecule), $N–1$ (radical cation) and $N+1$ (radical anion) electrons. The ρ^{HOMO}(r) and ρ^{LUMO}(r) are values of the electron densities of the HOMO and LUMO.

If Eqs. (3 and 4) are integrated for individual atoms in a molecule, one obtains the so-called condensed Fukui function (CFF) [68], which provides a more convenient way to predict the reaction site in the molecule. The condensed Fukui function for an atom, noted as A, can be written as:

$$f_{\mathrm{A}}^{-} = p_{N}^{\mathrm{A}} - p_{N-1}^{\mathrm{A}} \tag{6}$$

$$f_{\mathrm{A}}^{+} = p_{N}^{\mathrm{A}} - p_{N+1}^{\mathrm{A}} \tag{7}$$

where p_N^A is the electron population number of atom A. Since atomic charge is defined as $q^{\mathrm{A}}=Z^{\mathrm{A}}-p^{\mathrm{A}}$, where Z is the charge of atomic nucleus, f^- and f^+ can be expressed as the difference of atomic charges in two states (note that two Z terms are cancelled). By analogous treatment, one can easily formulate the CFFs for an atom A in Eqs. (8-10) for electrophilic, nucleophilic and radical attack:

$$f_{\mathrm{A}}^{+} = q_{N}^{\mathrm{A}} - q_{N+1}^{\mathrm{A}} \tag{8}$$

$$f_{\mathrm{A}}^{-} = q_{N-1}^{\mathrm{A}} - q_{N}^{\mathrm{A}} \tag{9}$$

$$f_{\mathrm{A}}^{0} = \left[q_{N-1}^{\mathrm{A}} - q_{N+1}^{\mathrm{A}} \right] / 2 \tag{10}$$

where q_N^{A}, q_{N-1}^{A}, and q_{N+1}^{A} are the NBO charges on atom A of the neutral, anionic and cationic species, respectively [70]. The three formulas 8-10 are exploited in this work to describe the electrophilic, nucleophilic and free-radical attack. The larger the value of the CFF at a reaction site, represents the greater the reactivity of that corresponding site towards reactive specie. The

CFFs were estimated from the NBO charges employing the equations 8-10. This method is often used for calculation of the CFFs (*f*) [70, 71, 72, 73].

The most probable sites for the electrophilic (f^-), nucleophilic (f^+), and radical attack (f^0) are given in Table S4. The NBO charges predicted that the C3, O2, N1, and C4" were the most reactive atoms both for electrophilic and free-radical attack. As for the nucleophilic attack, five positions were favored: C1', C4, O3, C7 and C4" (bold in Table S4). On the basis of the obtained CCF values for free radical attack, it is obvious that N1 and O2 atoms are the most reactive positions for hydrogen atom transfer (HAT) and/or sequential proton loss electron transfer SPLET mechanisms [74], while the C3 and C4" atoms are the most reactive sites for radical adduct formation (RAF) mechanism [75].

3.10. Molecular docking analysis

PASS (Prediction of Activity Spectra for Substances) is an online program designed as a tool for evaluating the general biological potential of an organic drug-like molecule. PASS provides simultaneous predictions of many types of biological activity based on the structure of the organic compounds [76-79]. PASS analysis of **1** predicted inhibition of Ubiquinol-Cytochrome C Reductase Binding Protein (UQCRB) and Methylenetetrahydrofolate reductase (MTHFR) with activities which values of Pa (probability to be active) were 0.802 and 0.794 (bold in Table 7). These two proteins were chosen because of their biological importance. UQCRB is involved in the transfer of electrons across the mitochondrial inner membrane and plays an important role in complex III stability. Recent research showed that down-regulation of this protein inhibits angiogenesis and suggested that UQCRB could be a novel therapeutic target

for angiogenesis regulation. Angiogenesis is a process responsible for embryonic development and tissue or organ regeneration. In pathological conditions, this process is important for progression of tumors and hepatic fibrosis. Applications of small bioactive molecules that bind to the UQCRB suppress hypoxia-induced tumor angiogenesis. This data demonstrates that UQCRB could be applied as a target agent in new approaches for human cancer and mitochondria-related disease [80]. MTHFR is a cytosolic enzyme, that catalyzes conversion of the N^5,N^{10}-methylentetrahydrofolate to N^5-methyltetrahydrofolate, the methyl donor for remethylation of the homocysteine to methionine [81]. Human and other eukaryotic MTHFR exist as a homodimer and each subunit (70-77 kDa) contains a catalytic domain and a regulatory domain. This enzyme plays an important role in the folic acid and homocysteine metabolism. Mutations in human MTHFR results in loss of enzyme activity and leads to high homocysteine and low folate levels in plasma. Homocysteine is an oxidant and play a vital role in oxidation of lipid and lipoproteins [82]. Elevated level of homocysteine concentration in plasma is associated with endothelial disfunction, platelet aggregation, and atherosclerosis.

To evaluate the inhibitory nature of **1** against UQCRB and MTHFR proteins, the molecular docking studies were performed. Protein-ligand binding energy and identification of the potential ligand binding sites were determined from this study as well. The ligand conformation which showed the lowest binding energy (best position) was determined based the ligand docking results. The position and orientation of ligand inside protein receptor and the interactions with amino acids which bound to the ligand were analyzed and visualized with Discovery Studio 4.0 and AutoDockTools.

Table 7. PASS prediction for the activity spectrum of 3-(1-(phenylamino)ethylidene)-chroman-2,4-dione.

Pa>0,7	Pi	Predicted activity
0.886	0.003	Cholestanetriol 26-monooxygenase inhibitor
0.858	0.022	Membrane integrity agonist
0.851	0.003	4-Nitrophenol 2-monooxygenase inhibitor
0.821	0.014	CYP2H substrate
0.811	0.004	CYP2B5 substrate
0.802	**0.018**	**Methylenetetrahydrofolate reductase (NADPH) inhibitor**
0.794	**0.035**	**Ubiquinol-cytochrome-c reductase inhibitor**
0.766	0.009	Oxidoreductase inhibitor
0.757	0.046	CYP2C12 substrate
0.754	0.004	P-benzoquinone reductase (NADPH) inhibitor
0.751	0.048	Aspulvinone dimethylallyltransferase inhibitor
0.744	0.035	Gluconate 2-dehydrogenase (acceptor) inhibitor
0.739	0.010	Nitrate reductase (cytochrome) inhibitor
0.728	0.005	CYP2A4 substrate
0.706	0.006	CYP2A11 substrate
0.705	0.007	General pump inhibitor

The values of the estimated free energy of binding and inhibition constant (*K*i) for investigated ligand in ten different conformations are given in Tables S5 and S6. By analyzing positions of active amino acids, it can be concluded that ligand binds to the catalytic site of substrates by weak non-covalent interactions. The most prominent are H-bonds, alkyl-π and π-π interactions. In primary structures of chains D and A molecules of lysine in positions 226 and 169, regardless of the conformation of the investigated ligand (Fig. 6), have predominant role as active sites of UQCRB and MTHFR proteins for inhibitory action, respectively. LYS226 forms H-bond (2.05 Å length) with C=O group of the ligand. LYS226 amino group is protonated at physiological pH values which makes it a good electrophile. PHE442 forms two weak π-π interactions with benzene and chroman rings. On other hand, LYS169 and HIS153 form hydrogen bonds of 2.47 and 2.77 Å with C=O groups of the ligand. Histidine has electron-rich NH group and it is suitable for nucleophilic attack. LEU106 forms weak alkyl-π interaction with benzene ring of the ligand (Fig. 6). The docking analysis proves that the most probable site for the electrophilic attack is O2, as determined by the Fukui functions and high negative NBO charge. Out of all electronegative elements, O3 has the highest probability for nucleophilic attack, which additionally explains the important interaction formed between this atom and HIS153.

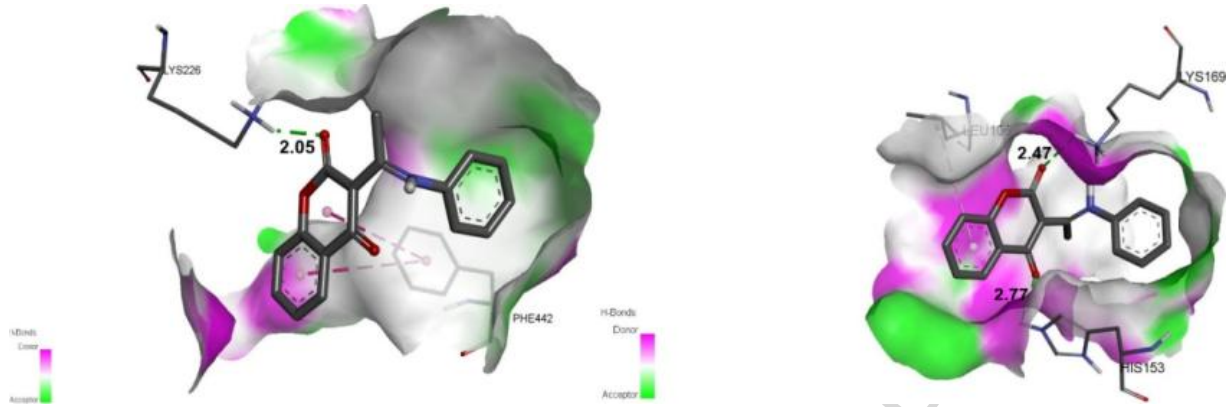

Figure 6. Picture showing interaction between ligand (conformation **1** of molecule **1**, the lowest *Ki*) and amino acids in Ubiquinol-Cytochrome C Reductase Binding Protein (UQCRB, left) and Methylenetetrahydrofolate reductase (MTHFR, right). The most important interaction distances (bold) are given in angstrom (Å).

4. Conclusions

The experimental and theoretical study of the structure of the synthesized coumarin derivative 3-(1-(phenylamino)ethylidene)-chroman-2,4-dione (**1**), is carried out. The selected DFT model (B3LYP-D3BJ/6–311+G(d,p)) almost perfectly reproduces the bond lengths and bond angles of the molecule. Calculated geometric parameters are in good agreement with crystal structures. The B3LYP-D3BJ functional also quite well reproduces spectroscopic characteristics of the molecule. The obtained values of the natural charge distribution are in accordance with MEPS data. The analysis of vibrational spectra gives very good agreement between the DFT method and the experimentally obtained results. The ^{1}H and ^{13}C NMR chemical shifts, obtained theoretically and experimentally, are in rather good accordance with correlation coefficients (R) moderately large and the mean absolute errors relatively small. The condensed Fukui functions are calculated for all atoms in title molecule by the means of NBO

charges. On the basis of the obtained these parameters, the most probable reactions sites for nucleophilic, electrophilic and free-radical attack were determined. The C3, O2, N1, and C4" atoms are favorable sites for electrophilic and free-radical attack, while the C1', C4, O3, C7 and C4" atoms are probable for nucleophilic attack.

To evaluate the inhibitory nature of compound **1** against UQCRB and MTHFR proteins, the molecular docking studies are performed. Results indicate that the ligand **1** forms a stable complex with UQCRB and MTHFR proteins, as evident from the binding energy (ΔG_{bind}, presented in Supplementary material). The most important interactions are H-bonds, π-π and π-alkyl. Atoms forming these bonds are predicted as the most reactive sites. Atoms forming bonds are predicted as the most reactive sites by the Fukui indices. These preliminary results suggest that the investigated ligand **1** might exhibit inhibitory activity against Ubiquinol-Cytochrome C Reductase Binding Protein and Methylenetetrahydrofolate reductase.

Acknowledgements: The authors are grateful to the Ministry of Education, Science and Technological Development of the Republic of Serbia (Projects Nos. OI172015, OI172016, and OI174028) for financial support. This work was further supported by the Ministry of Education, Science, Research and Sport of the Slovak Republic (Project VEGA No. 1/0598/14).

Supplementary data.

CCDC 1577270 contains the supplementary crystallographic data for **1**. These data can be obtained free of charge via http://www.ccdc.cam.ac.uk/conts/retrieving.html, or from the Cambridge Crystallographic Data Centre, 12 Union Road, Cambridge CB2 1EZ, UK; fax: (+44) 1223-336-033; or e-mail: deposit@ccdc.cam.ac.uk.

References

[1] B.D. Wagner, The Use of Coumarins as Environmentally-Sensitive Fluorescent Probes of Heterogeneous Inclusion Systems, Molecules 14 (2009) 210–237.

[2] C. Gleye, G. Lewin, A. Laurens, J.C. Jullian, P. Loiseau, C. Bories, R. Hocquemiller, Acaricidal activity of tonka bean extracts. Synthesis and structure-activity relationships of bioactive derivatives, J. Nat. Prod. 66 (2003) 690–692.

[3] J.R.S. Hoult, M. Payá, Pharmacological and biochemical actions of simple coumarins: Natural products with therapeutic potential, Gen. Pharmacol. 27 (1996) 713–722.

[4] J.A. Mead, J.N. Smith, R.T. Williams, Studies in detoxication. 72. The metabolism of coumarin and of o-coumaric acid, Biochem. J. 68 (1958) 67–74.

[5] S. Rosselli, A.M. Maggio, N. Faraone, V. Spadaro, S.L. Morris-Natschke, K.F. Bastow, K.-H. Lee, M. Bruno, The cytotoxic properties of natural coumarins isolated from roots of Ferulago campestris (Apiaceae) and of synthetic ester derivatives of aegelinol, Nat. Prod. Commun. 4 (2009) 1701–1706.

[6] T. Asao, G. Buchi, M.M. Abdel-Kader, S.B. Chang, E.L. Wick, G.N. Wogan, Aflatoxins B and G, J. Am. Chem. Soc. 85 (1963) 1706–1707.

[7] J.W. Hinman, E.L. Caron, H. Hoeksema, The Structure of Novobiocin 1, 2, J. Am. Chem. Soc. 79 (1957) 3789–3800.

[8] H. Raistrick, C.E. Stickings, R. Thomas, Studies in the biochemistry of microorganisms: Alternariol and alternariol monomethyl ether, metabolic products of Alternaria tenuis, Biochem. J. 55 (1953) 421–433.

[9] E. Lederer, Chemistry and biochemistry of some mammalian secretions and excretions, J. Chem. Soc. (1949) 2115-2125.

[10] B.P. Moore, Coumarin-like substances from Australian termites, Nature. 195 (1962) 1101–1102.

[11] M. Grazul, E. Budzisz, Biological activity of metal ions complexes of chromones, coumarins and flavones, Coord. Chem. Rev. 253 (2009) 2588–2598.

[12] V. Semeniuchenko, U. Groth, V. Khilya, Synthesis of Chroman-2-ones by Reduction of Coumarins, Synthesis 21 (2009) 3533-3556.

[13] A.M. El-Agrody, M.S. Abd El-Latif, N.A. El-Hady, A.H. Fakery, A.H. Bedair, Heteroaromatization with 4-Hydroxycoumarin Part II: Synthesis of Some New Pyrano[2,3-d]pyrimidines, [1,2,4]triazolo[1,5-c]pyrimidines and Pyrimido[1,6-b]-[1,2,4]triazine Derivatives, Molecules. 6 (2001) 519–527.

[14] S. Pratibha, P. Shreeya, Note Synthesis, characterization and antimicrobial studies of some novel 3-arylazo-7 -hydroxy-4- methylcoumarins, 38 (1999) 1139–1142.

[15] Z.M. Nofal, M.I. El-Zahar, S.S. Abd El-Karim, Novel coumarin derivatives with expected biological activity, Molecules 5 (2000) 99–113.

[16] C. Kontogiorgis, D. Hadjipavlou-Litina, Biological evaluation of several coumarin derivatives designed as possible anti-inflammatory/antioxidant agents, J. Enzyme Inhib. Med. Chem. 18 (2003) 63–69.

[17] G. Melagraki, A. Afantitis, O. Igglessi-Markopoulou, A. Detsi, M. Koufaki, C. Kontogiorgis, D.J. Hadjipavlou-Litina, Synthesis and evaluation of the antioxidant and anti-inflammatory activity of novel coumarin-3-aminoamides and their alpha-lipoic acid adducts, Eur. J. Med. Chem. 44 (2009) 3020–3026.

[18] D. Bhavsar, J. Trivedi, S. Parekh, M. Savant, S. Thakrar, A. Bavishi, A. Radadiya, H. Vala, J. Lunagariya, M. Parmar, L. Paresh, R. Loddo, A. Shah, Synthesis and in vitro anti-HIV

activity of N-1,3-benzo[d]thiazol-2-yl-2- (2-oxo-2H-chromen-4-yl)acetamide derivatives using MTT method, Bioorganic Med. Chem. Lett. 21 (2011) 3443–3446.

[19] C.A. Kontogiorgis, D.J. Hadjipavlou-Litina, Synthesis and antiinflammatory activity of coumarin derivatives, J. Med. Chem. 48 (2005) 6400–6408.

[20] X. He, Y.Y. Chen, J.B. Shi, W.J. Tang, Z.X. Pan, Z.Q. Dong, B.A. Song, J. Li, X.H. Liu, New coumarin derivatives: Design, synthesis and use as inhibitors of hMAO, Bioorganic Med. Chem. 22 (2014) 3732–3738.

[21] K. Aslam, M.K. Khosa, N. Jahan, S. Nosheen, Short communication: synthesis and applications of Coumarin, Pak. J. Pharm. Sci. 23 (2010) 449–454.

[22] M. Zabradnik, The Production and Application of Fluorescent Brightening Agent, John Wiley and Sons Ltd, New York, 1992.

[23] R.D.H. Murray, J. Mendez, S.A. Brown, The Natural Coumarins, Occurrence, Chemistry and Biochemistry, Wiley, New York,(c), Hatano T., Yasuhara T., Fukuda T., Noro T., Okuda T., Chem. Pharm. Bull. 37 (1989) 3005.

[24] M. Zahradník, Z. Procházka, The production and application of fluorescent brightening agents, John Wiley & Sons, New York, 1982.

[25] R. O'Kennedy, R.D. Thornes, Coumarins : biology, applications, and mode of action, John Wiley & Sons, New York 1997.

[26] P.J. Frosch, J.D. Johansen, T. Menne, C. Pirker, S.C. Rastogi, K.E. Andersen, M. Bruze, A. Goossens, J.P. Lepoittevin, I.R. White, Further important sensitizers in patients sensitive to fragrances. II. Reactivity to essential oils, Contact Dermatitis 47 (2002) 279–287.

[27] D.R. Ilić, V.V. Jevtić, G.P. Radić, K. Arsikin, B. Ristić, L.J. Harhaji-Trajković, N. Vuković, S. Sukdolak, O. Klisurić, V. Trajković, S.R. Trifunović, Synthesis,

characterization and cytotoxicity of a new palladium(II)complex with a coumarine-derived ligand, Eur. J. Med. Chem. 74 (2014) 502-508.

[28] G. Uray, O.S. Wolfbeis, H. Junek, β,β-Diacyl enamines and enols. IV. A proton NMR and UV spectroscopic study of β,β-diacyl enamino groups, J. Mol. Struct. 54 (1979) 77-88.

[29] S. Sukdolak, N. Vuković, S. Solujić, N. Manojlović, Lj. Krstić, Hantzsch reaction of 3-(2-bromoacetyl)-4-hydroxy-chromen-2-one. Synthesis of 3-(thiazol-4-yl)-4-hydroxy coumarines, J. Heterocycl. Chem. 41 (2004) 593–596.

[30] Oxford Diffraction, CrysAlis CCD, CCD Data Collection GUI. Oxford Diffraction Ltd. Oxford, UK (2007).

[31] G.M. Sheldrick, SHELXT – Integrated space-group and crystal-structure determination, Acta Crystallogr. Sect. A Found. Adv. 71 (2015) 3–8.

[32] G.M. Sheldrick, Crystal structure refinement with SHELXL, Acta Crystallogr. Sect. C Struct. Chem. 71 (2015) 3–8.

[33] L.J. Farrugia, WinGX suite for small-molecule single-crystal crystallography, J. Appl. Crystallogr. 32 (1999) 837–838.

[34] A.L. Spek, Structure validation in chemical crystallography, Acta Crystallogr. Sect. D Biol. Crystallogr. 65 (2009) 148–155.

[35] K. Brandenburg, DIAMOND, Crystal Impact GbR, Bonn, Germany, 2007 (2012).

[36] M.J. Frisch, G.W. Trucks, H.B. Schlegel, G.E. Scuseria, M.A. Robb, J.R. Cheeseman, G. Scalmani, V. Barone, B. Mennucci, G.A. Petersson, H. Nakatsuji, M. Caricato, X. Li, H.P. Hratchian, A.F. Izmaylov, J. Bloino, G. Zheng, J.L. Sonnenberg, M. Hada, M. Ehara, K. Toyota, R. Fukuda, J. Hasegawa, M. Ishida, T. Nakajima, Y. Honda, O. Kitao, H. Nakai, T. Vreven, J. A. Montgomery, Jr., J.E. Peralta, F. Ogliaro, M. Bearpark, J.J. Heyd, E.

Brothers, K.N. Kudin, V.N. Staroverov, R. Kobayashi, J. Normand, K. Raghavachari, A. Rendell, J.C. Burant, S.S. Iyengar, J. Tomasi, M. Cossi, N. Rega, J.M. Millam, M. Klene, J.E. Knox, J.B. Cross, V. Bakken, C. Adamo, J. Jaramillo, R. Gomperts, R.E. Stratmann, O. Yazyev, A.J. Austin, R. Cammi, C. Pomelli, J.W. Ochterski, R.L. Martin, K. Morokuma, V.G. Zakrzewski, G.A. Voth, P. Salvador, J.J. Dannenberg, S. Dapprich, A.D. Daniels, Ö. Farkas, J.B. Foresman, J.V. Ortiz, J. Cioslowski, D.J. Fox, Gaussian 09, Revision D.1, Inc, Wallingford CT, 2013.

[37] A.D. Becke, Density-functional exchange-energy approximation with correct asymptotic behavior, Phys. Rev. A. 38 (1988) 3098–3100.

[38] A.D. Becke, Density-functional thermochemistry. III. The role of exact exchange, J. Chem. Phys. 98 (1993) 5648.

[39] A.D. Becke, E.R. Johnson, A density-functional model of the dispersion interaction, J. Chem. Phys. 123 (2005) 154101.

[40] E.R. Johnson, A.D. Becke, Van der Waals interactions from the exchange hole dipole moment: Application to bio-organic benchmark systems, Chem. Phys. Lett. 432 (2006) 600–603.

[41] S. Grimme, J. Antony, S. Ehrlich, H. Krieg, A consistent and accurate ab initio parametrization of density functional dispersion correction (dft-d) for the 94 elements H-Pu, J. Chem. Phys. 132 (2010) 154104.

[42] S. Grimme, S. Ehrlich, L. Goerigk, Effect of the damping function in dispersion corrected density functional theory, J. Comput. Chem. 32 (2011) 1456–1465.

[43] M. Sardo, R. Siegel, S.M. Santos, Combining multinuclear high-resolution solid-state MAS NMR and computational methods for resonance assignment of glutathione tripeptide, J. Rocha, J.R.B. Gomes, L. Mafra, J. Phys. Chem. A 116 (2012) 6711–6719.

[44] P. Ivanov, Performance of some DFT functionals with dispersion on modeling of the translational isomers of a solvent-switchable [2]rotaxane, J. Mol. Struct. 1107 (2016) 31–38.

[45] R.A. Munos, Y.N. Panchenko, G.S. Koptev, N.F. Stepanov, Program for calculating distribution of potential energy in internal coordinates, J. Appl. Spectrosc. 12 (1970) 428–429.

[46] C.R. Legler, N.R. Brown, R.A. Dunbar, M.D. Harness, K. Nguyen, O. Oyewole, W.B. Collier, Scaled Quantum Mechanical Scale Factors for Vibrational Calculations using Alternate Polarized and Augmented Basis Sets with the B3LYP Density Functional Calculation Model, Spectrochim. Acta Part A 145 (2015) 15-24.

[47] A.V. Marenich, C.J. Cramer, D.G. Truhlar, Universal solvation model based on solute electron density and on a continuum model of the solvent defined by the bulk dielectric constant and atomic surface tensions, J. Phys. Chem. B 113 (2009) 6378–6396.

[48] K. Wolinski, J.F. Hinton, P. Pulay, Efficient implementation of the gauge-independent atomic orbital method for NMR chemical shift calculations, J. Am. Chem. Soc. 112 (1990) 8251–8260.

[49] J.E. Carpenter, F. Weinhold, Analysis of the geometry of the hydroxymethyl radical by the "different hybrids for different spins" natural bond orbital procedure, J. Mol. Struc. THEOCHEM 169 (1988) 41–62.

[50] A.E. Reed, L.A. Curtiss, F. Weinhold, Intermolecular interactions from a natural bond orbital, donor-acceptor viewpoint, Chem. Rev. 88 (1988) 899–926.

[51] G.M. Morris, R. Huey, W. Lindstrom, M.F. Sanner, R.K. Belew, D.S. Goodsell, A.J. Olson, AutoDock4 and AutoDockTools4: Automated docking with selective receptor flexibility, J. Comput. Chem. 30 (2009) 2785-2791.

[52] Y. Sun, X. Zhang, W. Xie, G. Liu, X. He, Y. Huang, G. Zhang, J. Wang, Z. Kuang, R. Zhang, Identification of UQCRB as an oxymatrine recognizing protein using a T7 phage display screen, J. Ethnopharmacol. 193 (2016) 133–139.

[53] S. Igari, A. Ohtaki, Y. Yamanaka, Y. Sato, M. Yohda, M. Odaka, K. Noguchi, K. Yamada, Properties and Crystal Structure of Methylenetetrahydrofolate Reductase from Thermus thermophilus HB, PLoS One. 6 (2011) e23716.

[54] J. Bernstein, R.E. Davis, L. Shimoni, N.-L. Chang, Patterns in Hydrogen Bonding: Functionality and Graph Set Analysis in Crystals, Angew. Chemie Int. Ed. English. 34 (1995) 1555–1573.

[55] G. Gilli, F. Bellucci, V. Ferretti, V. Bertolasi, Evidence for resonance-assisted hydrogen bonding from crystal-structure correlations on the enol form of the .beta.-diketone fragment, J. Am. Chem. Soc. 111 (1989) 1023–1028.

[56] M. Małecka, S.J. Grabowski, E. Budzisz, Crystal and molecular structures of 3-[1-(2-hydroxyethylamino)-ethylidene]-chroman-2,4-dione and 2-methoxy-3-[1-(benzylamino)-ethylidene]-2,3-dihydro-2,4-dioxo-2λ5-benzo[e][1,2]oxaphosphinane and DFT study of intramolecular H-bonds of related compounds, Chem. Phys. 297 (2004) 235–244.

[57] E.H. Avdović, D.L.J. Stojković, V.V. Jevtić, M. Kosić, B. Ristić, L. Harhaji-Trajković, M. Vukić, N. Vuković, Z.S. Marković, I. Potočňák, S.R. Trifunović, Synthesis,

characterization and cytotoxicity of a new palladium(II) complex with a coumarin-derived ligand 3-(1-(3-hydroxypropylamino)ethylidene)chroman-2,4-dione. Crystal structure of the 3-(1-(3-hydroxypropylamino)ethylidene)-chroman-2,4-dione, Inorganica Chim. Acta. 466 (2017) 188–196.

[58] D.L. Stojković, V.V. Jevtić, N. Vuković, M. Vukić, I. Potočňák, I.R. Zelen, M.M. Zarić, M.M. Mišić, D. Baskić, G.N. Kaluđerović, S.R. Trifunović, Crystal and molecular structure of a new palladium(II) complex with a coumarin-valine derivate, J. Struct. Chem. 58 (2017) 550–557.

[59] M. Małecka, E. Budzisz, 3-[(1-Benzylamino)ethylidene]-2 H -chromene-2,4(3 H)-dione, Acta Crystallogr. Sect. E Struct. Reports Online. 62 (2006) o5058–o5060.

[60] A. Brahmia, T. Ben Ayed, R. Ben Hassen, 3-[1-(2-Hydroxyanilino)ethylidene]-3 H -chromen-2,4-dione, Acta Crystallogr. Sect. E Struct. Reports Online. 69 (2013) o1296–o1296.

[61] C.R. Groom, I.J. Bruno, M.P. Lightfoot, S.C. Ward, The Cambridge structural database, Acta Crystallogr. Sect. B Struct. Sci. Cryst. Eng. Mater. 72 (2016) 171–179.

[62] E.H. Avdović, D. Milenković, J.M. Dimitrić-Marković, N. Vuković, S.R. Trifunović, Z. Marković, Structural, spectral and NBO analysis of 3-(1-(3-hydroxypropylamino) ethylidene) chroman-2, 4-dione, J. Mol. Struct. 1147 (2017) 69-75.

[63] S. Chidangil, M.K. Shukla, P.C. Mishra, A Molecular Electrostatic Potential Mapping Study of Some Fluoroquinolone Anti-Bacterial Agents, J. Mol. Model. 4 (1998) 250–258.

[64] F.J. Luque, J.M. López, M. Orozco, Perspective on Electrostatic interactions of a solute with a continuum. A direct utilization of ab initio molecular potentials for the prevision of solvent effects, Theor. Chem. Acc. 103 (2000) 343–345.

[65] D.M. Burland, R.D. Miller, C.A. Walsh, Second-order nonlinearity in poled-polymer systems, Chem. Rev. 94 (1994) 31–75.

[66] R.G. Parr, W. Yang, Density functional approach to the frontier-electron theory of chemical reactivity, J. Am. Chem. Soc. 106 (1984) 4049–4050.

[67] L.I.U. Shu-BIN, Conceptual Density Functional Theory and Some Recent Developments, Acta Phys. Chim Sin. 25 (2009) 590–600.

[68] W. Yang, W.J. Mortier, The use of global and local molecular parameters for the analysis of the gas-phase basicity of amines, J. Am. Chem. Soc. 108 (1986) 5708–5711.

[69] R.G. Parr, R.G. Pearson, Absolute hardness: companion parameter to absolute electronegativity, J. Am. Chem. Soc. 105 (1983) 7512–7516.

[70] L. Senthilkumar, P. Kolandaivel, Study of effective hardness and condensed Fukui functions using AIM, ab initio, and DFT methods, Mol. Phys. 103 (2005) 547–556.

[71] W. Tiznado, E. Chamorro, R. Contreras, P. Fuentealba, Comparison among four different ways to condense the Fukui function, J. Phys. Chem. A. 109 (2005) 3220–3224.

[72] T. Mineva, E. Sicilia, N. Russo, Density-functional approach to hardness evaluation and its use in the study of the maximum hardness principle, J. Am. Chem. Soc. 120 (1998) 9053-9058.

[73] G. De Luca, E. Sicilia, N. Russo, T. Mineva, On the hardness evaluation in solvent for neutral and charged systems, J. Am. Chem. Soc. 124 (2002) 1494-1499.

[74] D. Milenković, J. Đorović, S. Jeremić, J.M. Dimitrić Marković, E.H. Avdović, Z. Marković, Free radical scavenging potency of dihydroxybenzoic acids, J. Chem-NY 2017 (2017).

[75] A. Galano, M. Francisco-Marquez, Reactions of OOH radical with β-carotene, lycopene, and torulene: hydrogen atom transfer and adduct formation mechanisms, J. Phys. Chem. B. 113 (2009) 11338–11345.

[76] R.K. Goel, D. Singh, A. Lagunin, V. Poroikov, PASS-assisted exploration of new therapeutic potential of natural products, Med. Chem. Res. 20 (2011) 1509–1514.

[77] N. Khurana, M.P.S. Ishar, A. Gajbhiye, R.K. Goel, PASS assisted prediction and pharmacological evaluation of novel nicotinic analogs for nootropic activity in mice, Eur. J. Pharmacol. 662 (2011) 22–30.

[78] P. Tiwari, B. Kumar, M. Kaur, G. Kaur, H. Kaur, Phytochemical screening and extraction: a review, Int. Pharm. Sci. 1 (2011) 98–106.

[79] A. Hasanat, M.S.H. Kabir, M.M. Hossain, M. Hasan, M.A.A. Masum, T.A. Chowdhury, D.I. Bhuiyan, A. Mamur, A. Kibria, Antibacterial activity of methanol extract of macaranga denticulata leaves and in silico pass prediction for its six secondary metabolites, World J. Pharm. Sci. 3 (2015) 1258–1266.

[80] Y.S. Cho, H.J. Jung, S.H. Seok, A.Y. Payumo, J.K. Chen, H.J. Kwon, Functional inhibition of UQCRB suppresses angiogenesis in zebrafish, Biochem. Biophys. Res. Commun. 433 (2013) 396–400.

[81] D.S. Rosenblatt, Identification of UQCRB as an oxymatrine recognizing protein using a T7 phage display screen, Clin. Invest. Med. 24 (2001) 56–59.

[82] K. Yamada, Z. Chen, R. Rozen, R.G. Matthews, Effects of common polymorphisms on the properties of recombinant human methylenetetrahydrofolate reductase, Proc. Natl. Acad. Sci. U. S. A. 98 (2001) 14853–14858.

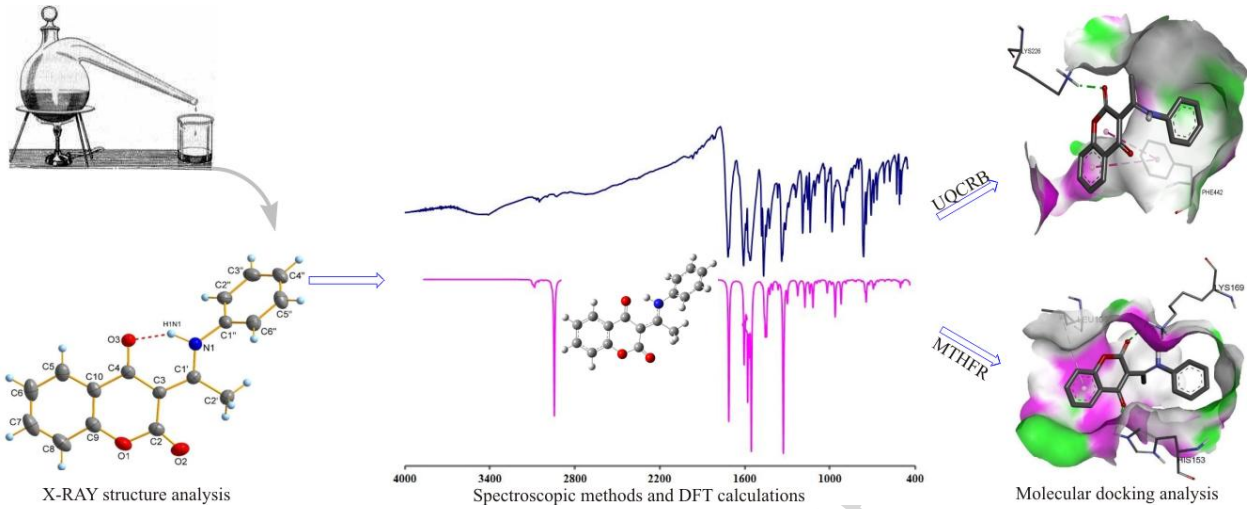

Graphical abstract

Highlights

- X-ray structure analysis and spectroscopic methods are utilized.
- The structure and spectroscopic behavior of the **1** were determined by DFT.
- The Fukui functions are used for predict the reaction site in a molecule.
- Molecular docking analysis evaluated the inhibitory nature of **1.**